High-field magnetoelectric and spin-lattice coupling in multiferroic $(NH_4)_2[FeCl_5{\cdot}(H_2O)]$

Kendall D. Hughey,[†] Minseong Lee,[‡] Jisoo Nam,[¶] Amanda J. Clune,[†] Kenneth R. O'Neal,[†] Wei Tian,[§] Randy S. Fishman,[‖] Mykhaylo Ozerov,[⊥] JunHee Lee,[¶] Vivien S. Zapf,[‡] and Janice L. Musfeldt[*,†,#]

†*Department of Chemistry, University of Tennessee, Knoxville, Tennessee 37996, USA*

‡*National High Magnetic Field Laboratory, Los Alamos National Laboratory, Los Alamos, New Mexico 87545, USA*

¶*School of Energy and Chemical Engineering, Ulsan National Institute of Science and Technology, Ulsan 44919, Korea*

§*Neutron Scattering Division, Oak Ridge National Laboratory, Oak Ridge, Tennessee 37831, USA*

‖*Materials Science and Technology Division, Oak Ridge National Laboratory, Oak Ridge, Tennessee 37831, USA*

⊥*National High Magnetic Field Laboratory, Tallahassee, Florida, 32310, USA*

#*Department of Physics, University of Tennessee, Knoxville, Tennessee 37996, USA*

E-mail: musfeldt@utk.edu

Abstract

We combine high field polarization, magneto-infrared spectroscopy, and lattice dynamics calculations with prior magnetization to explore the properties of $(NH_4)_2[FeCl_5 \cdot (H_2O)]$ - a Type II molecular multiferroic in which the mixing between charge, structure, and magnetism is controlled by through-space hydrogen- and halogen-bonds. Electric polarization is sensitive to the series of field-induced spin reorientations, increasing linearly with field and reaching a maximum before collapsing to zero across the quasi-collinear to collinear-sinusoidal reorientation due to the restoration of inversion symmetry. Magnetoelectric coupling is on the order of 1.2 ps/m for the $P \| c$, $H \| c$ configuration between 5 and 25 T at 1.5 K. In this range, the coupling takes place via an orbital hybridization mechanism. Other forms of mixing are active in $(NH_4)_2[FeCl_5 \cdot (H_2O)]$ as well. Magneto-infrared spectroscopy reveals that all of the vibrational modes below 600 cm^{-1} are sensitive to the field-induced transition to the fully saturated magnetic state at 30 T. We analyze these local lattice distortions and use frequency shifts to extract spin-phonon coupling constants for the Fe–O stretch, Fe–OH_2 rock, and NH_4^+ twist. Inspection also reveals subtle symmetry breaking of the ammonium counterions across the ferroelectric transition. The coexistance of such varied mixing processes in a platform with intermolecular hydrogen- and halogen-bonding opens the door to greater understanding of multiferroics and magnetoelectrics governed by through-space interactions.

Introduction

Single phase materials that fully couple ferroelectricity and ferromagnetism have been challenging to realize due to the exacting combination of ultra-low symmetries required. While Type I multiferroics trigger electric and spin orders independently, Type II systems host inversion symmetry breaking magnetic order.[1] The latter is the most effective avenue to robust magnetoelectric coupling. Many materials offer tunable routes to broken spatial inversion and time reversal symmetries,[1–4] although complete (100%) magnetoelectric coupling depends upon inversion symmetry breaking magnetic orders and facile routes for creating electric dipoles. Molecule-based materials offer these opportunities in abundance. They retain many of the same physical characteristics as the oxides while offering lower energy scales, tunable chemical architectures, flexible lattices, and rich phase diagrams.[5–12] This makes molecule-based multiferroics like $[(CH_3)_2NH_2]Mn(HCOO)_3$, $Cu(CH_3)_2SOCl_2$, and $Cu(pyz)(gly)ClO_4$ superb platforms for exploring unique states of matter away from equilibrium.[5,13–17] Others including κ-(BEDT-TTF)$_2$Cu[N(CN)$_2$]Cl and $NiCl_2$–$4SC(NH_2)_2$ are wholly molecular in nature with through-space interactions that provide both electric and magnetic functionality.[18,19] In this work, we build upon recent magnetization and neutron scattering work on multiferroic $(NH_4)_2[FeCl_5\cdot(H_2O)]$[20–25] with a combination of high field electric polarization, magneto-infrared spectroscopy, and first principles lattice dynamics calculations. By so doing, we provide a framework for understanding the interplay between charge, structure, and magnetism in this system.

$(NH_4)_2[FeCl_5\cdot(H_2O)]$ is the multiferroic member of the $A_2[BX_5\cdot(H_2O)]$ family of erythrosiderites (A = K^+, Rb^+, NH_4^+; B = Fe^{3+}, Mn^{3+}, Co^{3+}; X = Cl^-, Br^-, H_2O). In this system, $[FeCl_5(H_2O)]^{2-}$ groups are arranged in a herringbone-like pattern along the b-axis [Fig. 1 (a)]. The overall structure is governed by an extensive network of intermolecular hydrogen- and halogen- bonding.[20,26–29] Ammonium (NH_4^+) fills the anion pocket and balances charge. This material is magnetically complex with five unique but nearly iso-energetic exchange pathways (J_{1-5}), all of which are associated with various types of OH$\cdots$Cl and

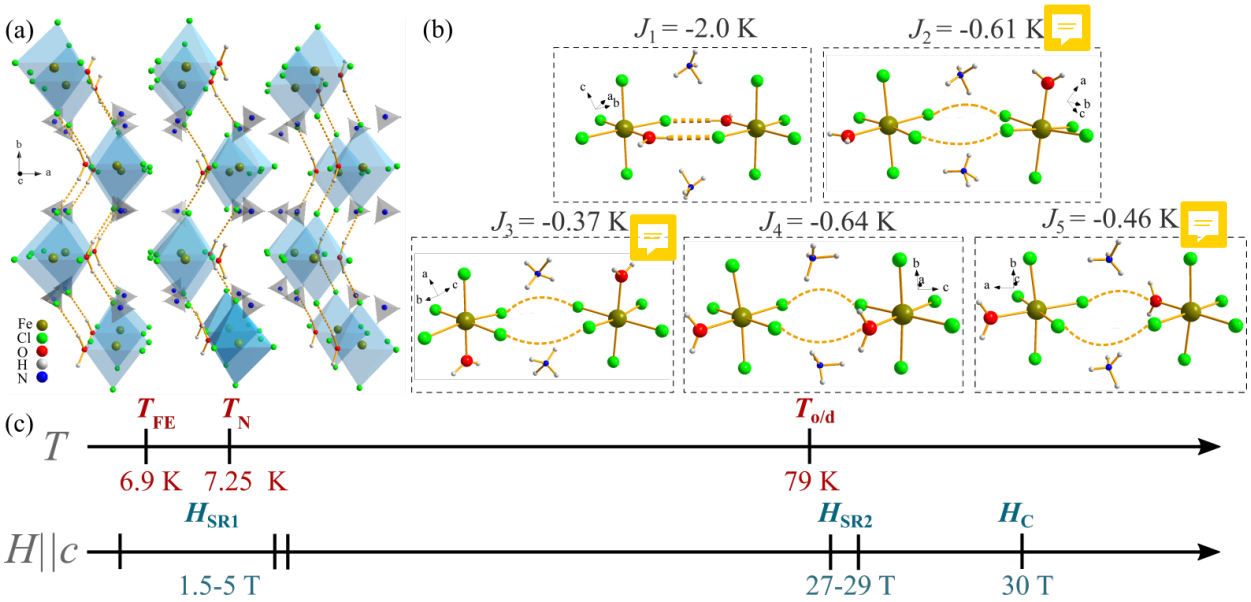

Figure 1: (a) Crystal structure of $(NH_4)_2[FeCl_5{\cdot}(H_2O)]$ at room temperature.[20] The primary hydrogen-bonding interactions (arising from J_1) yield herringbone-like connectivity. (b) Summary of the five exchange pathways mediated by hydrogen- and halogen-bonding. The strength of each pathway is indicated. These values are determined from fits to the neutron scattering data.[25] J_1 involves purely hydrogen bonds with a O-H$\cdots$Cl pathway, J_2 and J_3 have Cl$\cdots$Cl interactions, and J_4 and J_5 have asymmetric pathways with one Cl$\cdots$O and one Cl$\cdots$Cl pathway.[26–28] Weak interactions between the H centers of the ammonium counterion and the Cl and O ions are also present.[26,27,29] A single J Hamiltonian is employed, and the negative sign indicates antiferromagnetic interactions. The in-plane anisotropy D is 0.17 K.[25] (c) Summary of temperature- and field-driven transitions. $T_{o/d}$ is the order/disorder transition, T_N is the Néel transition, and T_{FE} is the ferroelectric transition temperature, respectively. Under magnetic field, there is a series of low field spin reorientations between 1 and 5 T that we refer to as H_{SR1}. H_{SR2} and H_C are the high-field spin reorientations between 27 and 29 T and saturation field, respectively.

Cl$\cdots$Cl interactions [Fig. 1 (b)].[7,20,26–29] The NH_4^+ counterions contribute to these through-space interactions. $(NH_4)_2[FeCl_5{\cdot}(H_2O)]$ displays a series of temperature-driven transitions [Fig. 1 (c)] including an order-disorder transition at 79 K,[30] magnetic ordering of the S = 5/2 Fe^{3+} centers below T_N = 7.25 K that creates a collinear sinusoidal spin wave structure with K = (0, 0, 0.23),[20,26] and ferroelectricity below T_{FE} = 6.9 K that arises due to the development of an incommensurate-cycloidal spin state (K_1 = (0 0 0.23) that coexists (and competes) with a commensurate distorted cycloidal phase K_2 = (0 0 0.25)).[20,23] Modeling of the inelastic neutron scattering reveals that J_2 and J_4 are the source of frustration and

responsible for the cycloidal character of the spin waves.[25] Numerical simulation shows that in-plane magnetic anisotropies within the plane as well as geometrical frustration in the exchange interactions stabilizes the collinear sinusoidal phase.[31] $(NH_4)_2[FeCl_5{\cdot}(H_2O)]$ is a Type II system.[1] Multiferroicity arises from an inverse Dzyaloshinskii-Moriya (spin-current) mechanism in which the spin cycloid breaks inversion symmetry.[4,32] The microscopic nature of the lattice distortion that creates electric polarization is not known at the present time.

Under magnetic field, $(NH_4)_2[FeCl_5{\cdot}(H_2O)]$ undergoes a series of frustration-induced spin reorientations between 1 and 5 T.[20,21] Several high field spin reorientations take place before the transition to the fully saturated magnetic state at $H_C = 30$ T as well [Fig. 1 (c)].[21] Spin density calculations reveal how intermolecular interactions support magnetic exchange and how these pathways change across the transition to the fully saturated state.[21] Electric polarization is closely linked to magnetization. In fact, the series of low field spin reorientations trigger polarization flops (from a to a' and a' to c) as well as changes in the elastic response at 5 T.[20] Multiferroicity in the commensurate quasi-collinear state ($K_3 = 0\ 0\ 0$) above 5 T is described by the spin-dependent p-d hybridization model.[32] Thus, there are two distinct magnetoelectric coupling mechanisms in the same material (inverse Dzyaloshinskii-Moriya between 0 and 5 T and p-d hybridization above 5 T) rather than a single overarching mechanism. This situation is unexpected and merits investigation. To our knowledge, a field-dependent magnetoelectric coupling mechanism is observed in only one other material.[?] In any case, the non-collinear spin structure and ferroelectric phases are rather fragile - a finding reinforced by potassium substitution studies in $[(NH_4)_{1-x}K_x][FeCl_5{\cdot}(H_2O)]$.[33] Magnetoelectric and magnetoelastic coupling at higher fields are wholly unexplored - a process made all the more intriguing by the presence of a field dependent magnetoelectric mechanism.

Inspired by the discovery of complex spin-charge interactions in a purely molecular multiferroic, we combined several techniques that are rarely brought together - high-field polarization, magneto-infrared spectroscopy, first principles lattice dynamics calculations, and magnetization[21] - to uncover magnetoelectric and spin-phonon interactions in $(NH_4)_2[FeCl_5{\cdot}(H_2O)]$.

We demonstrate that this system is indeed a multiferroic with strong magnetoelectric coupling with peaks in the magnetoelectric current at the significant phase boundaries. We find a maximum ΔP of 19 μC/m^2 near 24 T and deterministic control of this quantity between approximately 5 and 25 T due to systematic spin canting. The magnetoelectric coupling constant α_{me} is on the order of 1.2 ps/m for the $P\|c$, $H\|c$ configuration between 5 and 25 T at 1.5 K. This interaction derives from orbital hybridization. In a dramatic demonstration of how inversion symmetry impacts the properties of a Type II multiferroic, polarization plunges to zero across the field-driven quasi-collinear $\rightarrow$ collinear sinusoidal magnetic orientation transition, and it remains flat across the 30 T magnetic saturation transition due to the restoration of the inversion center. At the same time, we show that other forms of cross-coupling - in addition to magnetoelectric interactions - are active in $(NH_4)_2[FeCl_5{\cdot}(H_2O)]$. Magneto-infrared spectroscopy reveals spin-phonon coupling involving the majority of low-frequency modes across the magnetic quantum phase transition. The librational modes involving ammonium and water have the largest amplitude changes whereas the Fe–O stretch and Fe-OH_2 rock have the most sizeable coupling constants. We also employ the magneto-infrared spectra to uncover subtle symmetry breaking of the ammonium counterions across the ferroelectric phase transition. These findings demonstrate how charge, structure, and magnetism mix using only through-space hydrogen- and halogen-bonding to create strongly coupled functionalities in an ultra-low symmetry molecular multiferroic.

Results and discussion

Magnetoelectric coupling across the magnetically-driven transitions

Figure 2 summarizes the magnetoelectric properties of $(NH_4)_2[FeCl_5{\cdot}(H_2O)]$ in the $P||c$, $H||c$ configuration. Similar results in other measurement configurations are given in Supplementary Information. Figure 2 (a,b) highlights the change in electric polarization ΔP as a function of magnetic field (up- and down-sweeps) at temperatures both above and below

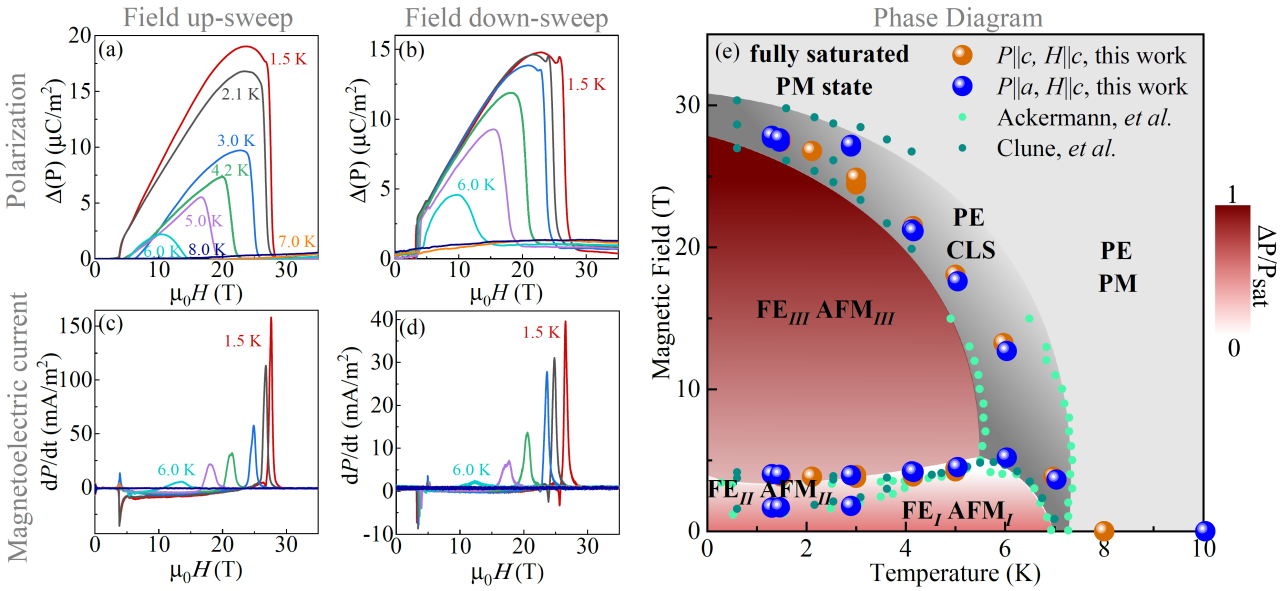

Figure 2: (a,b) Change in electric polarization (ΔP) of $(NH_4)_2[FeCl_5{\cdot}(H_2O)]$ as a function of magnetic field (up- and down-sweeps) at various temperatures. This is the $P||c$, $H||c$ configuration. Others are given in Supplementary Information. In each case, polarization is measured after poling the sample in an electric field. (c,d) Magnetoelectric current I=dP/dt vs. applied field, highlighting changes in $\Delta P(H)$. (e) H-T phase diagram of $(NH_4)_2[FeCl_5{\cdot}(H_2O)]$ derived from the magnetization[21] along with points taken from our magnetoelectric current measurements. The latter are indicated as orange ($P||c, H||c$) and blue ($P||a, H||c$) spheres. Here, FE=ferroelectric, PE=paraelectric, AFM=antiferromagnetic, CLS=collinear sinusoidal, and PM=paramagnetic. A color bar is included to indicate the size of ΔP.

$T_{\rm FE}$ = 6.9 K. At low fields, ΔP is zero, consistent with prior work.[20] This finding indicates that polarization lies primarily within the ab plane (9° off of the a-axis) in zero field.[20] A polarization flop to the c-axis is responsible for the sharp rise near 5 T.[20] We find that ΔP rises above the spin flop transition, increasing almost linearly with field in the ferroelectric state. At base temperature, ΔP reaches a maximum of 19.03 μC/m^2 near 24 T at 1.5 K, starts to decrease slightly, and then plunges to zero near 27 T. This is consistent with a Type II mechanism in which magnetic order breaks inversion symmetry.[1] The overall magnitude of ΔP is smaller at 4 K, and the collapse occurs at significantly lower magnetic field than in the 1.5 K data. The 6 K curve shows modest signatures of this transition as well, but the effects are smeared because this shot was taken in close proximity to the triple point. By contrast, ΔP is zero in the dielectric phase.

Figure 2 (c,d) displays the magnetoelectric current, I=dP/dt, as a function of applied field. Sharp peaks in the magnetoelectric current denote the exact position of each transition. The fact that peaks in the magnetoelectric current coincide with magnetically-driven transitions[20,21] demonstrates that $(NH_4)_2[FeCl_5{\cdot}(H_2O)]$ is a high field multiferroic. As a reminder, the correspondence of high field electric polarization and magnetic transitions is evidence of magnetoelectric coupling, while the fact that poling controls the sign of the electric polarization provides evidence for ferroelectricity and thus multiferroic behavior. We extract a magnetoelectric coupling constant from our data as $\alpha_{me} = (\partial P/\partial H)_T$. We find that α_{me} is 1.2 ps/m for the $P\|c$, $H\|c$ configuration between 5 and 25 T at 1.5 K - comparable with that in other multiferroics.

Within the $p-d$ hybridization mechanism,[34?] the electric polarization induced by charge transfer from a metal ion with spin $\mathbf{S}$ to the ligand along vector $\mathbf{e}$ is proportional to $(\mathbf{e}\cdot\mathbf{S})\,\mathbf{S}$. We apply this result to the high field spin-flop phase assuming that $\mathbf{e}$ points between the coupled Fe ions. Then, the predicted electric polarization for field along either the a- or c-axis is proportional to $\mathbf{c}\sin 2\theta$, where θ is the tilting angle of the spins from the c-axis due to the magnetic field. Since $\sin\theta \propto H$, the induced polarization increases linearly with field for small θ. For field along both a and c, the electric polarization is indeed dominated by the c component. We would expect that the polarization along c reaches a maximum when $\theta = \pi/4$ or when the magnetization equals about 70% of its saturation value, in rough agreement with our measurements. Rather than mediated by a single ligand, however, each magnetic coupling between Fe ions is mediated by two O$\cdots$Cl or Cl$\cdots$Cl linkages. Nevertheless, this model does correctly predict that the electric polarization in the spin-flop phase is a linear function of magnetic field in the c direction [Fig. 2(a)] and that it reaches a maximum before decreasing again.[?] It also predicts that the response along a is zero above 5 T, which is also observed (Supplemental Information).

Bringing these polarization results together with prior magnetization work,[20,21] we develop a magnetic field - temperature (H–T) phase diagram that summarizes the behavior

of both charge and spin as well as the interaction between electric polarization and the spin arrangement [Fig. 2 (e)]. That polarization flops from a to c across the cycloidal $\rightarrow$ quasi-collinear magnetic transition at 5 T is an excellent demonstration of how the charge and spin channels interact in the low field regime. As expected, the 5 T transition is observed in both the $P||c$, $H||c$ and $P||a$, $H||c$ data sets; the 1.5 K transition ($P||a' \rightarrow P||a''$) is only detected when $P||a$. The high field behavior of $(NH_4)_2[FeCl_5{\cdot}(H_2O)]$ provides an even more foundational demonstration of Type II multiferroicity and magnetoelectric coupling. Polarization trends are not correlated with the 30 T magnetic saturation transition as one might naively expect. Instead, ΔP plunges to zero across the magnetic reorientation transition near 27 T - evidence that the microscopic spin configuration has changed in a fundamental manner - despite the fact that the magnetic moment itself continues to grow. The fact that ΔP goes to zero at the quasi-collinear to collinear-sinusoidal spin transition reveals that inversion symmetry is restored due to the development of a collinear state. Here, we can equate ΔP with P because $P = 0$ outside the inversion symmetry-breaking magnetic phases. These results along with low field neutron diffraction work[30,32] suggests that all of the magnetic states above 27 T (including the fully saturated state) are likely to be collinear. In other words, the $K_2 = (0\ 0\ 0.25)$ phase, which is the commensurate distorted cycloid phase, does not persist above 5 T. We also see that while inverse Dzyaloshinskii-Moriya and p-d hybridization models account for magnetoelectric coupling at zero and low fields, respectively, $(NH_4)_2[FeCl_5{\cdot}(H_2O)]$ maintains an orbital hybridization mechanism at the highest fields.

Magneto-infrared response of multiferroic $(NH_4)_2[FeCl_5{\cdot}(H_2O)]$

Infrared spectroscopy and vibrational mode assignments

$(NH_4)_2[FeCl_5{\cdot}(H_2O)]$ is well-studied in the infrared, although previous investigations focus primarily on vibrational motions of water-coordinated aquo-complexes en masse and how the pattern varies with counterion substitution (K^+, Rb^+, NH_4^+).[35–37] For the most part, prior efforts address the behavior of the fundamental excitations of the lattice above 350 cm^{-1}.[35–38]

Our interests are different and instead concentrate on the development of magnetoelectricity and the behavior of the lattice across the sequence of temperature and field-driven transitions. Furthermore, we focus primarily on the low-frequency vibrational modes [Fig. 3 (a)]. The Fe-Cl stretch at 276 cm^{-1}, the Fe-O stretch at 365 cm^{-1}, and the Fe-OH_2 stretch at 420 cm^{-1} are of particular interest in this work. They are assigned based upon our lattice dynamics calculations. There are several important low-frequency librational, torsional, and wagging motions of NH_4^+ and H_2O as well. The NH_4^+-related features are located mostly below 200 cm^{-1}, the water wag is at 185 cm^{-1}, and a prominent H_2O libration is near 450 cm^{-1}.[35,36,38] A full set of assignments as well as a complete discussion of temperature trends across the 79 K order-disorder and 6.9 K ferroelectric transitions is available in Supplementary Information.

Spin-phonon coupling across the magnetic saturation transition

Figure 3 (a) summarizes the magneto-infrared response of $(NH_4)_2[FeCl_5 \cdot (H_2O)]$ across the 30 T transition to the fully saturated state. In addition to absolute absorption at zero and 35 T, we also show a full field absorption difference curve $\Delta\alpha = \alpha(35\ T) - \alpha(0\ T)$, which serves to emphasize small spectral changes under magnetic field. Remarkably, and without exception, all lattice distortions below 600 cm^{-1} are sensitive to applied magnetic field whereas those above this frequency are completely rigid. This behavior is entirely different from that of the copper halide coordination polymers like $Cu(pyz)(NO_3)_2$ or $[Cu(pyz)_2(2\text{-}HOpy)_2](PF_6)_2$ where only one or two vibrational modes are sensitive to the magnetically-driven phase transition.[39,40] Normalizing the absorption difference data as $\Delta\alpha(35\ T)/\alpha(0\ T)$ allows us to evaluate the magnitude of these effects. The majority of local lattice distortions change by less than 10% in a 35 T magnetic field, although several of the lowest frequency modes reveal much larger field-induced modifications – up to 46% [Fig. 3 (b)]. These motions are highly collective in nature and involve NH_4^+ counterion librations.[35,36,38] Displacement patterns for two characteristic distortions are included in the inset.

In order to quantify these effects, we integrate the absolute value of the absorption dif-

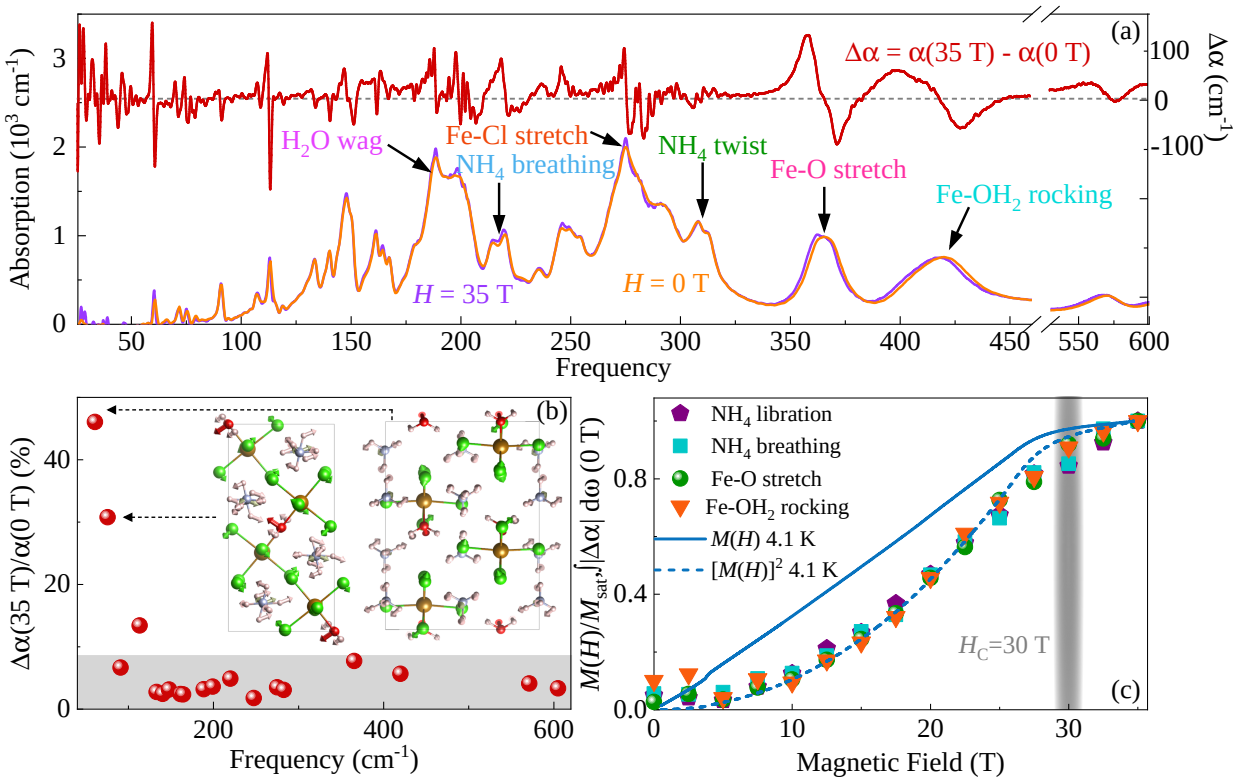

Figure 3: (a) Absorption spectrum of $(NH_4)_2[FeCl_5{\cdot}(H_2O)]$ at 0 and 35 T focusing on the low-frequency regime along with the full field absorption difference spectrum, $\Delta\alpha = \alpha(35\ \mathrm{T})$ - $\alpha(0\ \mathrm{T})$. Data are taken at 4.2 K. All vibrational modes in this region are magneto-active whereas those above 600 cm^{-1} are completely rigid. (b) Analysis of the percent changes in low-frequency phonons across the magnetic ~~quantum~~ phase transition, along with calculated displacement patterns of two characteristic H_2O ligand and NH_4^+ counterion librations. (c) Comparison of the integrated area of the absorption difference spectra for several different magneto-active vibrations along with the low-temperature magnetization[21] and the square of magnetization. The critical field, where the spins are fully saturated, is indicated in gray.

ference over an appropriate frequency window $\int |\Delta\alpha| \mathrm{d}\omega$ and plot these results as a function of magnetic field. In this way, we can reveal how specific local lattice distortions correlate with the development of the magnetic state. Figure 3 (c) displays the integrated absorption differences of several important vibrational modes along with the low temperature magnetization[21] and the square of magnetization. $\int |\Delta\alpha| \mathrm{d}\omega$ starts small and reaches a plateau as the magnetization saturates. All modes track $[M(H)]^2$ remarkably well, demonstrating that the local lattice distortions are sensitive to the microscopic nature of the spin state.[39,41,42] That said, it is the magnetic saturation transition at 30 T, not the myriad of weaker spin

reorientations evident in the H-T phase diagram[21] or loss of the inversion center above 27 T, that governs spin-phonon coupling in $(NH_4)_2[FeCl_5{\cdot}(H_2O)]$.

We evaluate spin-phonon coupling across the magnetically-driven phase transition at 30 T as $\omega = \omega_0 + \lambda\langle S_i \cdot S_j\rangle$ where ω and ω_0 are the perturbed and unperturbed phonon frequencies, λ is the mode-dependent spin-phonon coupling constant, and $\langle S_i \cdot S_j\rangle$ is the nearest-neighbor spin-spin correlation function. The magnitude of λ gives insight into how the magnetic exchange interaction J is modulated by the various phonon displacements.[43,44] Using the limiting low temperature value of $\langle S_i \cdot S_j\rangle = S^2 = (5/2)^2 = 6.25$, we calculate λ for several important distortions including the Fe-O stretch, the Fe-OH_2 rocking mode, and the NH_4 twist. These values are summarized in Table 1. The coupling constant for the two Fe-containing modes is on the order of 0.3 cm^{-1}, and that of the ammonium twist is an order of magnitude lower. These values are significantly smaller than the coupling constants of other molecule-based materials such as the low-dimensional copper halides across their magnetic saturation transitions.[44] We attribute the difference to: (i) through-space hydrogen- and halogen-bond exchange pathways in $(NH_4)_2[FeCl_5{\cdot}(H_2O)]$ as compared with super-exchange pathways created by metal$\cdots$ligand$\cdots$metal linkages in low-dimensional quantum magnets and (ii) the value of the spin ($S = 5/2$ for Fe^{3+} vs. $1/2$ for Cu^{2+}) which determines the size of the spin-spin correlation function.

Table 1: Summary of the coupling processes in $(NH_4)_2[FeCl_5{\cdot}(H_2O)]$ along with the overall size of each effect and mechanisms. Here, α_{me} and λ are the magnetoelectric and spin-phonon coupling constants, respectively.

Type of coupling	Overall size	Coupling mechanism
Magnetoelectric coupling	19 $\mu C/m^2$ (24 T, $P\|\|c$ $H\|\|c$, 1.5 K) α_{me} = 1.2 ps/m (5 - 25 T)	Spin-charge interaction $\alpha_{me} = (\partial P/\partial H)_T$ $\approx(\Delta P/\Delta H)_T$
Spin-lattice interaction	λ = -0.30 for Fe-O stretch λ = -0.34 for Fe-OH_2 rocking λ = -0.04 NH_4 for twist	Spin-phonon coupling $\omega = \omega_0 + \lambda\langle S_i \cdot S_j\rangle$

Local lattice distortions in the ferroelectric state

In order to uncover local lattice distortions across the ferroelectric transition, we examined the infrared response of $(NH_4)_2[FeCl_5{\cdot}(H_2O)]$ as a function of temperature with special attention to spectral changes near $T_{FE} = 6.9$ K. Unfortunately, there are surprisingly strong thermal contraction effects - even at low temperature - which obscure any spectral changes across the ferroelectric transition. This makes the overall results of such an analysis inconclusive [Fig. S3]. Since large thermal contraction effects preclude a straightforward identification of the polar modes, we turn to high field spectroscopy. As a reminder, the ferroelectric transition is triggered by a magnetic transition in a Type II multiferroic. Thus, lattice distortions due to ferroelectricity in $(NH_4)_2[FeCl_5{\cdot}(H_2O)]$ can (in principle) be revealed through an analysis of spectral changes across the field-driven ferroelectric $\leftrightarrow$ paraelectric transition. Magneto-infrared changes are significantly smaller here but uncontaminated by thermal contraction [Fig. S4]. Moreover spectral changes thus obtained ignore certain differences in magnetic state and are at the limit of our sensitivity. It is, however, still possible to carry out an analysis. We find a number of features below 300 cm^{-1} that are sensitive to the development of ferroelectricity. These are primarily ammonium counterion librations.[33,45–48] This finding is consistent with recent spin density calculations predicting that through-space hydrogen- and halogen-bonding interactions depend upon the magnetic state.[21] A full analysis is presented in the Supplementary Information [Figs. S3 and S4].

Summary and outlook

We combine high field electric polarization, magneto-infrared spectroscopy, and lattice dynamics calculations with prior magnetization to explore the properties of $(NH_4)_2[FeCl_5{\cdot}(H_2O)]$. This molecular multiferroic is held together entirely by hydrogen- and halogen-bonds and, as a result of the overall low energy scales, is extraordinarily sensitive to external stimuli. Electric polarization grows linearly with increasing field, reaching a maximum near 24 T,

and plunges to zero as the inversion center is lost near 27 T - consistent with expectations for a Type II multiferroic. We extract a magnetoelectric coupling constant on the order of 1.2 ps/m for the $P\|c$, $H\|c$ configuration between 5 and 25 T at 1.5 K. This value of α_{me} is comparable with what is found in other multiferroics. We also analyze the electric polarization and magnetoelectric current in terms of predictions for the *p*-*d* hybridization mechanism and show the coupling between metal ions by two different ligand pathways produces an electric polarization that remains a linear function of the magnetic field up to nearly the point when the magnetization reaches 70% of its saturation value. Combining these findings with prior magnetization work deepens the overall understanding of the competing states of matter in the magnetic field - temperature phase diagram. The fundamental excitations of the lattice are well integrated in this system. Magneto-infrared spectroscopy reveals that all of the vibrational modes below 600 cm^{-1} are sensitive to the field-induced transition to the fully saturated magnetic state. This is in striking contrast to many other molecule-based materials in which only a few local lattice distortions aid in the development of the fully saturated spin state. We analyze these findings in terms of spin-phonon coupling across the magnetically-driven transition at 30 T and extract coupling constants for the Fe-O stretch and Fe-OH_2 rocking modes on the order of -0.3 cm^{-1}. That of the NH_4^+ twist is an order of magnitude smaller. These distortions modify through-space hydrogen- and halogen-bonding pathways and, as a result, the superexchange interactions. We also employ changes in the magneto-infrared response to reveal distortions of the ammonium counterions across the ferroelectric transition. These effects are extremely subtle and involve NH_4^+ librations. The coexistence of charge-spin-lattice mixing processes in $(NH_4)_2[FeCl_5{\cdot}(H_2O)]$ suggests that other external stimuli such as pressure or strain will be useful for modulating properties as well.

Methods

Crystal growth and sample preparation: Large $(NH_4)_2[FeCl_5 \cdot (H_2O)]$ single crystals were obtained using solution techniques with HCl, $FeCl_3$, and NH_4Cl as starting materials - similar to the method reported previously.[20] The saturated solution was kept at 38 °C in an environment chamber to allow slow evaporation. The crystals are sensitive to air, so they were stored in a dry box. Crystal orientation was determined using the well-developed flat surfaces: [1 0 0], [2 1 0], [1 0 1], and [0 1 1]. Surfaces were polished to reveal specific faces for polarization measurements. Capacitor plates were attached with Ag paint, and vacuum grease was used to mount the crystals onto the probe tip. For the infrared work, the sample was mixed with paraffin or KBr for far and middle infrared spectroscopy, respectively. This allows control of optical density. Where necessary, the samples were mounted on pinholes with rubber cement.

Polarization measurements: Pulsed-field polarization was measured in two different ways: (i) by poling the sample while cooling in 100 V from above T_N to the final measurement temperature and then removing the electric field before measuring $P(H)$ and (ii) by poling the sample as above and then leaving the electric field on while measuring $P(H)$. The first method proves that $(NH_4)_2[FeCl_5 \cdot (H_2O)]$ is a ferroelectric since the electric polarization remains even after the electric field is removed. The data obtained from the second method yields a larger electric polarization - making it easier to identify each phase transitions. We found similar results using both protocols. We can control the sign of the electric polarization by the direction of the poling field. The magnetoelectric current was measured by recording the change in surface charge on parallel capacitor plates applied with silver paint to the crystalline surface, using a SR570 current to voltage amplifier during a milisecond magnetic field pulse.[49] We integrated the measured magnetoelecric current with time to obtain the change in polarization $\Delta P(H)$. In order to remove any background signatures, we subtracted the 10 K polarization curve (which is well above the ferroelectric ordering temperature) from

the low-temperature curves.

Magneto-infrared spectroscopy: We employed a series of Fourier transform infrared spectrometers (20-5000 cm^{-1}, 2 cm^{-1} resolution) to measure the infrared vibrational response of $(NH_4)_2[FeCl_5 \cdot (H_2O)]$. Absorption was calculated as $\alpha(\omega) = -\frac{1}{hd} ln[\mathcal{T}(\omega)]$ where h is the concentration, d is the thickness, and $\mathcal{T}(\omega)$ is the measured transmittance. An open flow helium cryostat (4.2-300 K) provided temperature control. Magneto-infrared spectroscopy was performed at the National High Magnetic Field Laboratory in Tallahassee, FL using a 35 T resistive magnet. In order to emphasize small spectral changes with magnetic field, we calculate absorption differences as $\Delta\alpha = \alpha(\omega, H) - \alpha(\omega, H = 0\ T)$. We quantify these results by integrating the absorption difference over an appropriate frequency window: $\int |\Delta\alpha| d\omega$. The limits of integration vary for each phonon.

Theoretical approach: First-principles calculations were performed using DFT within the local density approximation LDA + U method as implemented in the Vienna ab initio simulation package (VASP 5.4.1).[50–52] The Dudarev implementation[53] with on-site Coulomb interaction U = 2.0 eV was used to treat the localized 3d electron states in Fe. Our value for U is chosen to bring Q closest to the experimental value. The projector augmented wave (PAW) potentials[54,55] explicitly include eight valence electrons for Fe ($3d^7 4s^1$), five for N ($2s^3 2p^3$), one for H ($1s^1$), seven for Cl ($3s^2 3p^5$), and six for O ($2s^2 2p^4$). The experimental crystal structure at 2 K was used as the initial structure[27] and then optimized for both lattice parameters and atomic positions with collinear-antiferromagnetic spin ordering. A plane-wave basis set with a cutoff energy of 500 eV was used. The k-point sampling used the Monkhorst–Pack[56] scheme and employed $4 \times 6 \times 8$ mesh for structure optimization and IR calculation of $(NH_4)_2[FeCl_5 \cdot (H_2O)]$ unit cell. The atomic positions were optimized until the interatomic forces were smaller than 1 meV/Å. DFPT linear response calculation and Born effective charges are used to obtain infrared intensities.[57–64]

Acknowledgement

Research at Tennessee is supported by the National Science Foundation (DMR-1707846). A portion of this work was performed at the National High Magnetic Field Laboratory, which is supported by National Science Foundation Cooperative Agreement No. DMR-1644779 and the State of Florida. V.S.Z., W.T. and R.S.F. acknowledge funding from the U.S. Department of Energy, Office of Science, Basic Energy Sciences, Materials Sciences and Engineering Division, Condensed Matter Experiment and Theory Programs. J.H.L. and J.N. at UNIST were supported by Basic Research Laboratory (NRF2017R1A4A1015323), Creative Materials Discovery Program (2017M3D1A1040828) of NRF, the MOTIE (Ministry of Trade, Industry and Energy) (No. 10080657) and KRSC (Korea Semiconductor Research Consortium) support program. We thank Mark Turnbull for useful conversations.

Supporting Information Available

Supplementary information accompanies the paper. Relevant data includes magnetic field-induced polarization in other P/H configurations, tabulated vibrational mode assignments, a discussion of spectral changes across the order-disorder transition, and analyses of local lattice distortions across the ferroelectric transition.

References

(1) Khomskii, D. Classifying multiferroics: mechanisms and effects. *Physics* **2009**, *2*, 20.

(2) Vecchini, C.; Chapon, L. C.; Brown, P. J.; Catterji, T.; Park, S.; Cheong, S.-W.; Radaelli, P. G. Commensurate magnetic structures of $R\mathrm{Mn_2O_5}$(R=Y,Ho,Bi) determined by single-crystal neutron diffraction. *Physical Review B* **2008**, *77*, 134424.

(3) Cheong, S.-W.; Mostovoy, M. Multiferroics: a magnetic twist for ferroelectricity. *Nature Materials* **2007**, *6*, 13–20.

(4) Tokura, Y.; Seki, S.; Nagaosa, N. Multiferroics of spin origin. *Reports on Progress in Physics* **2014**, *77*, 076501.

(5) Jain, P.; Ramachandran, V.; Clark, R. J.; Zhou, H. D.; Toby, B. H.; Dalal, N. S.; Kroto, H. W.; Cheetham, A. K. Multiferroic behavior associated with an order-disorder hydrogen bonding transition in metal-organic frameworks (MOFs) with the perovskite ABX_3 architecture. *Journal of the American Chemical Society* **2009**, *131*, 13625–13627.

(6) Jain, P.; Stroppa, A.; Nabok, D.; Marino, A.; Rubano, A.; Paparo, D.; Matsubara, M.; Nakotte, H.; Fiebig, M.; Picozzi, S.; Choi, E. S.; Cheetham, A. K.; Draxl, C.; Dalal, N. S.; Zapf, V. S. Switchable electric polarization and ferroelectric domains in a metal-organic-framework. *npj Quantum Materials* **2016**, *1*, 16012.

(7) Gómez-Aguirre, L. C.; Pato-Doldán, B.; Mira, J.; Castro-García, S.; Senarís-Rodríguez, M. A.; Sánchez-Anduújar, M.; Singleton, J.; Zapf, V. S. Magnetic ordering-induced multiferroic behavior in $[CH_3NH_3][Co(HCOO)_3]$ metal-organic framework. *Journal of the American Chemical Society* **2015**, *138*, 1122–1125.

(8) Pardo, E.; Train, C.; Liu, H.; Chamoreau, L. M.; Dkhil, B.; Boubekeur, K.; Lloret, F.; Nakatani, K.; Tokoro, H.; Ohkoshi, S. I.; Verdaguer, M. Multiferroics by rational design: implementing ferroelectricity in molecule-based magnets. *Angewandte Chemie - International Edition* **2012**, *51*, 8356–8360.

(9) Cai, H. L.; Zhang, Y.; Fu, D. W.; Zhang, W.; Liu, T.; Yoshikawa, H.; Awaga, K.; Xiong, R. G. Above-room-temperature magnetodielectric coupling in a possible molecule-based multiferroic: triethylmethylammonium tetrabromoferrate(III). *Journal of the American Chemical Society* **2012**, *134*, 18487–18490.

(10) Cañadillas-Delgado, L.; Fabelo, O.; Rodríguez-Velamazán, J. A.; Lemée-Cailleau, M. H.; Mason, S. A.; Pardo, E.; Lloret, F.; Zhao, J. P.; Bu, X. H.; Simonet, V.; Colin, C. V.; Rodríguez-Carvajal, J. The role of order-disorder transitions in the quest for molecular multiferroics: structural and magnetic neutron studies of a mixed valence iron(II)-iron(III) formate framework. *Journal of the American Chemical Society* **2012**, *134*, 19772–19781.

(11) Bosch-Serrano, C.; Clemente-Juan, J. M.; Coronado, E.; Gaita-Ariño, A.; Palii, A.; Tsukerblat, B. Molecular analog of multiferroics: electric and magnetic field effects in many-electron mixed-valence dimers. *Physical Review B* **2012**, *86*, 024432.

(12) Wu, S. Y. Applications of Raman microscopy for spin-phonon coupling and magnon excitation study in nanocrystals. *Current Microscopy Contributions to Advances in Science and Technology* **2012**, *3*, 1036–1043.

(13) Zapf, V. S.; Kenzelmann, M.; Wolff-Fabris, F.; Balakirev, F.; Chen, Y. Magnetically induced electric polarization in an organometallic magnet. *Physical Review B* **2010**, *82*, 060402(R).

(14) Stroppa, A.; Barone, P.; Jain, P.; Picozzi, S. Hybrid improper ferroelectricity in a multiferroic and magnetoelectric metal-organic framework. *Advanced Materials* **2013**, *25*, 2284–2290.

(15) Clune, A.; Hughey, K.; Lee, C.; Abhyankar, N.; Ding, X.; Dalal, N.; Whangbo, M.-H.; Singleton, J.; Musfeldt, J. Magnetic field-temperature phase diagram of multiferroic $[(CH_3)_2NH_2]Mn(HCOO)_3$. *Physical Review B* **2017**, *96*, 104424.

(16) Lancaster, T. et al. Controlling magnetic order and quantum disorder in molecule-based magnets. *Physical Review Letters* **2014**, *112*, 207201.

(17) Brambleby, J. et al. Combining microscopic and macroscopic probes to untangle the

single-ion anisotropy and exchange energies in an S=1 quantum antiferromagnet. *Physical Review B* **2017**, *95*, 234435.

(18) Lunkenheimer, P.; Müller, J.; Krohns, S.; Schrettle, F.; Loidl, A.; Hartmann, B.; Rommel, R.; De Souza, M.; Hotta, C.; Schlueter, J. A.; Lang, M. Multiferroicity in an organic charge-transfer salt that is suggestive of electric-dipole-driven magnetism. *Nature Materials* **2012**, *11*, 755–758.

(19) Zapf, V. S.; Sengupta, P.; Batista, C. D.; Nasreen, F.; Wolff-Fabris, F.; Paduan-Filho, A. Magnetoelectric effects in an organometallic quantum magnet. *Physical Review B* **2011**, *83*, 140405(R).

(20) Ackermann, M.; Brüning, D.; Lorenz, T.; Becker, P.; Bohatý, L. Thermodynamic properties of the new multiferroic material $(NH_4)_2[FeCl_5(H_2O)]$. *New Journal of Physics* **2013**, *15*, 123001.

(21) Clune, A. J.; Nam, J.; Lee, M.; Hughey, K. D.; Tian, W.; Fernandez-Baca, J. A.; Fishman, R. S.; Singleton, J.; Lee, J. H.; Musfeldt, J. L. Magnetic field-temperature phase diagram of multiferroic $(NH_4)_2$FeCl5$\cdot H_2O$. *npj Quantum Materials* **2019**, *44*, 4.

(22) Tian, W.; Cao, H.; Wang, J.; Ye, F.; Matsuda, M.; Yan, J.-Q.; Liu, Y.; Garlea, V. O.; Agrawal, H. K.; Chakoumakos, B. C.; Sales, B. C.; Fishman, R. S.; Fernandez-Baca, J. A. Spin-lattice coupling mediated multiferroicity in $(ND_4)_2FeCl_5\cdot D_2O$. *Physical Review B* **2016**, *94*, 214405.

(23) Tian, W.; Cao, H. B.; Clune, A. J.; Hughey, K. D.; Hong, T.; Yan, J.-Q.; Agrawal, H. K.; Singleton, J.; Sales, B. C.; Fishman, R. S.; Musfeldt, J. L.; Fernandez-Baca, J. A. Electronic phase separation and magnetic-field-induced phenomena in molecular multiferroic $(ND_4)_2FeCl_5\cdot D_2O$. *Physical Review B* **2018**, *98*, 054407.

(24) Alberto Rodríguez-Velamazán, J.; Fabelo, O.; Millán, A.; Campo, J.; Johnson, R. D.;

Chapon, L. Magnetically-induced ferroelectricity in the $(ND_4)_2[FeCl_5(D_2O)]$ molecular compound. *Scientific Reports* **2015**, *5*, 14475.

(25) Bai, X.; Fishman, R. S.; Sala, G.; Pajerowski, D. M.; Garlea, V. O.; Hong, T.; Lee, M.; Fernandez-Baca, J. A.; Cao, H.; Tian, W. Magnetic excitations of the hybrid multiferroic $(ND_4)_2[FeCl_5(D_2O)]$, submitted to Physical Review B.

(26) McElearney, J. N.; Merchant, S. Nonisomorphic antiferromagnetic behavior of two isomorphic salts: low-temperature heat capacities and magnetic susceptibilities of $(NH_4)_2FeCl_5{\cdot}H_2O$ and $K_2FeCl_5{\cdot}H_2O$. *Inorganic Chemistry* **1978**, *17*, 1207–1215.

(27) Figgis, B. N.; Raston, C. L.; Sharma, R. P.; White, A. H. Crystal structure of diammonium aquapentachloroferrate(III). *Australian Journal of Chemistry* **1978**, *31*, 2717–2720.

(28) Campo, J.; Luzón, J.; Palacio, F.; McIntyre, G. J.; Millán, A.; Wildes, A. R. Understanding magnetic interactions in the series $A_2FeX_5H_2O$ (A=K, Rb; X=Cl, Br). II. Inelastic neutron scattering and DFT studies. *Physical Review B* **2008**, *78*, 054415.

(29) Schultz, A. J.; Carlin, R. L. Single-crystal pulsed neutron diffraction structure of the antiferromagnet $K_2[FeCl_5(H_2O)]$ with and without applied pressure. *Acta Crystallographica Section B* **1995**, *51*, 43–47.

(30) Rodríguez-Velamazán, J. A.; Fabelo, Ó.; Millán, Á.; Johnson, R. D.; Chapon, L. Magnetically-induced ferroelectricity in the $(ND_4)_2[FeCl_5(D_2O)]$ molecular compound. *Scientific Reports* **2015**, *5*, 14475.

(31) Lee, M., **2021** arXiv:2103.08500.

(32) Rodríguez-Velamazán, J. A.; Fabelo, O.; Campo, J.; Millán, Á.; Rodríguez-Carvajal, J.; Chapon, L. C. Magnetic-field-induced change of magnetoelectric coupling in the hybrid multiferroic $(ND_4)_2[FeCl_5{\cdot}D_2O]$. *Physical Review B* **2017**, *95*, 174439.

(33) Brüning, D.; Fröhlich, T.; Langenbach, M.; Leich, T.; Meven, M.; Becker, P.; Bohatý, L.; Grüninger, M.; Braden, M.; Lorenz, T. Magnetoelectric coupling in the mixed erythrosiderite $[(NH_4)_{1x}K_x]_2[FeCl_5(H_2O)]$. *Physical Review B* **2020**, *102*, 054413.

(34) Jia, C.; Onoda, S.; Nagaosa, N.; Han, J. H. Microscopic theory of spin-polarization coupling in multiferroic transition metal oxides. *Physical Review B* **2007**, *76*, 144424.

(35) Adams, M.; Lock, P. J. A survey study of the vibrational spectra of some aquo-halogeno-complexes. *Journal of the Chemical Society A: Inorganic, Physical, Theoretical* **1971**, 2801–2806.

(36) Falk, M.; Huang, C.-H. Infrared studies of water in crystalline hydrates: $K_2FeCl{\cdot}H_2O$ (erythrosiderite) and related aquopentachloroferrates(III). *Canadian Journal of Chemistry* **1974**, *55*, 1736–1744.

(37) Sharma, S. K.; Pandya, D. K. Laser-Raman spectra of crystalline $(NH_4)FeCl_5{\cdot}H_2O$, $K_2FeCl_5{\cdot}$ H_2O and $K_2FeCl_5{\cdot}D_2O$. *Journal of Inorganic and Nuclear Chemistry* **1974**, *36*, 1165–1166.

(38) Lacková, D.; Ondrejkovičová, I.; Koman, M. A new pathway of preparation and refined structure of $(NH_4)_2[FeCl_5(H_2O)]$. *Acta Chimica Slovaca* **2013**, *6*, 129–132.

(39) Günaydin-Şen, O.; Lee, C.; Tung, L. C.; Chen, P.; Turnbull, M. M.; Landee, C. P.; Wang, Y. J.; Whangbo, M.-H.; Musfeldt, J. L. Spin-lattice interactions through the quantum critical transition in $Cu(pyz)(NO_3)_2$. *Physical Review B* **2010**, *81*, 104307.

(40) Hughey, K. D.; Clune, A. J.; Yokosuk, M. O.; Li, J.; Abhyankar, N.; Ding, X.; Dalal, N. D.; Xiang, H.; Smirnov, D.; Singleton, J.; Musfeldt, J. L. Structure-property relations in multiferroic $[(CH_3)_2NH_2]M(HCOO)_3$ (M=Mn, Co, Ni). *Inorganic Chemistry* **2018**, *57*, 11569–11577.

(41) Granado, E.; García, A.; Sanjurjo, J. A.; Rettori, C.; Torriani, I.; Prado, F.; Sánchez, R. D.; Caneiro, A.; Oseroff, S. B. Magnetic ordering effects in the Raman spectra of $La_{1-x}Mn_{1-x}O_3$. *Physical Review B* **1999**, *60*, 11879–11882.

(42) Al-Wahish, A.; O'Neal, K.; Lee, C.; Fan, S.; Hughey, K.; Yokosuk, M.; Clune, A.; Li, Z.; Schlueter, J.; Manson, J.; Whangbo, M.-H.; Musfeldt, J. Magnetic phase transitions and magnetoelastic coupling in $S = 1/2$ Heisenberg antiferromagnets. *Physical Review B* **2017**, *95*, 104437.

(43) Lee, J. H.; Rabe, K. M. Large spin-phonon coupling and magnetically induced phonon anisotropy in $SrMO_3$ perovskites (M=V,Cr,Mn,Fe,Co). *Physical Review B* **2011**, *84*, 104440.

(44) Hughey, K. D.; Harms, N. C.; O'Neal, K. R.; Clune, A. J.; Monroe, J. C.; Blockmon, A. L.; Landee, C. P.; Liu, Z.; Ozerov, M.; Musfeldt, J. L. Spin-lattice coupling across the magnetic quantum-phase transition in copper-containing coordination polymers. *Inorganic Chemistry* **2020**, *59*, 2127–2135.

(45) Ebisuzaki, Y. Raman spectra of NH_4Cl and NH_4Br: Dependence of the librational and the internal modes of the NH_4^+ ion on volume and on nitrogen-halogen distance. *The Journal of Chemical Physics* **1974**, *61*, 3170–3180.

(46) Boujelbene, M.; Mhiri, T. Vibrational spectra of $NH_4Sm(SO_4)_2{\cdot}4H_2O$ and $NH_4Ln(SO_4)_2{\cdot}2H_2O$[$Ln$=Yb,Tm]. *Journal of Solid State Chemistry* **1996**, *121*, 408–414.

(47) Prager, M.; Grimm, H.; Natkaniec, I.; Nowak, D.; Unruh, T. The dimensionality of ammonium reorientation in $(NH_4)_2S_2O_8$: The view from neutron spectroscopy. *Journal of Physics Condensed Matter* **2008**, *20*, 125218.

(48) Verdal, N.; Udovic, T. J.; Rush, J. J.; Stavila, V.; Wu, H.; Zhou, W.; Jenkins, T.

Low-temperature tunneling and rotational dynamics of the ammonium cations in $(NH_4)_2B_{12}H_{12}$. *Journal of Chemical Physics* **2011**, *135*, 094501.

(49) Chikara, S.; Singleton, J.; Bowlan, J.; Yarotski, D. A.; Lee, N.; Choi, H. Y.; Choi, Y. J.; Zapf, V. S. Electric polarization observed in single crystals of multiferroic Lu_2MnCoO_6. *Physical Review B* **2016**, *93*, 180405(R).

(50) Kresse, G.; Hafner, J. Ab *initio* molecular dynamics for liquid metals. *Physical Review B* **1993**, *47*, 558–561.

(51) Kresse, G.; Furthmüller, J. Efficient iterative schemes for ab initio total-energy calculations using a plane-wave basis set. *Physical Review B* **1996**, *54*, 11169–11186.

(52) Perdew, J. P.; Burke, K.; Ernzerhof, M. Generalized gradient approximation made simple. *Physical Review Letters* **1996**, *77*, 3865–3868.

(53) Dudarev, S.; Botton, G. Electron-energy-loss spectra and the structural stability of nickel oxide: an LSDA+U study. *Physical Review B* **1998**, *57*, 1505–1509.

(54) Blöchl, P. E. Projector augmented-wave method. *Physical Review B* **1994**, *50*, 17953–17979.

(55) Kresse, G.; Joubert, D. From ultrasoft pseudopotentials to the projector augmented-wave method. *Physical Review B* **1999**, *59*, 1758–1775.

(56) Pack, J. D.; Monkhorst, H. J. Special points for Brillouin-zone integrations. *Physical Review B* **1976**, *13*, 5188–5192.

(57) Gonze, X.; Lee, C. Dynamical matrices, Born effective charges, dielectric permittivity tensors, and interatomic force constants from density-functional perturbation theory. *Physical Review B* **1997**, *55*, 10355–10368.

(58) Gonze, X. Perturbation expansion of variational principles at arbitrary order. *Physical Review A* **1995**, *52*, 1086–1095.

(59) Karhánek, D.; Bučko, T.; Hafner, J. A density-functional study of the adsorption of methane-thiol on the (111) surfaces of the Ni-group metals: II. Vibrational spectroscopy. *Journal of Physics: Condensed Matter* **2010**, *22*, 265006.

(60) Pick, R. M.; Cohen, M. H.; Martin, R. M. Microscopic theory of force constants in the adiabatic approximation. *Physical Review B* **1970**, *1*, 910–920.

(61) Wu, X.; Vanderbilt, D.; Hamann, D. R. Systematic treatment of displacements, strains, and electric fields in density-functional perturbation theory. *Physical Review B* **2005**, *72*, 035105.

(62) Gajdoš, M.; Hummer, K.; Kresse, G.; Furthmüller, J.; Bechstedt, F. Linear optical properties in the projector-augmented wave methodology. *Physical Review B* **2006**, *73*, 045112.

(63) Karsch, F.; Patkós, A.; Petreczky, P. Phonons and related crystal properties from density-functional perturbation theory. *Reviews of Modern Physics* **2001**, *73*, 515–562.

(64) Gonze, X. DFPT: Adiabatic density-functional perturbation theory. *Physical Review A* **1995**, *52*, 1096–1114.

Graphical TOC entry

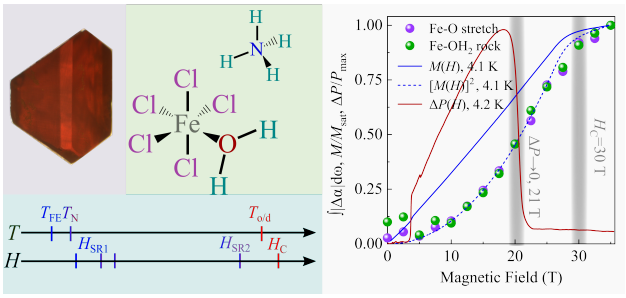

Figure 4: